

A review of derivative structures of the Miura-Ori

Chengrui Sui^{1,4,5}, Junlin Chen^{2,6}, Wenjie Jiang^{3,7}

¹Shanghai World Foreign Language Academy, Shanghai, 200233, China

²Shenzhen Senior High School, Shenzhen, 518038, China

³Yangcun Third Middle School, Tianjin, 301700, China

⁴Corresponding author

⁵horchsui@163.com

⁶3502964457@qq.com

⁷18822367091@163.com

Abstract. The scholarly paper conducts a thorough examination and evaluation of five primary derivatives of the Miura-Ori fold, a fundamental structure in the art of origami. Each derivative is meticulously studied through the creation of a tangible model, bringing the theoretical concepts to life. The space occupied by each model is precisely measured, providing a practical perspective to the study. These measurements are then compared and contrasted with the outcomes predicted by theoretical deductions, offering a comprehensive understanding of the accuracy of the theoretical models. The paper then transitions to encapsulate the most recent advancements and developments in the intriguing field of Miura-Ori folds. The potential applications of these primary derivatives are not limited to single-layered structures. The paper explores and deliberates on the exciting possibilities of utilizing these derivatives in multi-layered structures, opening up new avenues for practical applications. The paper concludes by charting the course for future research in this field.

Keywords: Miura-ori, Multi-layered, Origami

1. Introduction

Origami refers to the art of folding paper. It is of Japanese origin, a combination of the Japanese words ‘ori’, meaning folding and ‘kami’, meaning paper [1]. Origami works are widely appreciated in the fields of art and handicraft. The structures of origami patterns can also be applied in the design of deployable structures, as the process of folding up a paper into a product can be applied to the deployment of structures.

One of the most basic and widely used structures is the ‘miura-ori’, named after its inventor Kōryō Miura [2]. The fold is widely applied as it provides a path to fold a flat sheet of material into its compact form completely through motion in one direction, along the diagonal direction in the plane of the fully deployed plane. The folding pattern and the physical representation are shown in Fig. 1.a and Fig. 1.b, respectively.

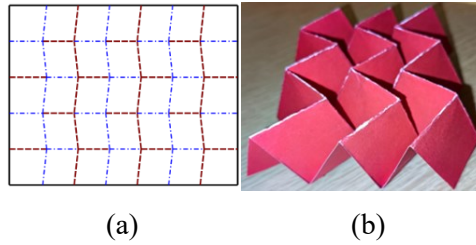


Figure 1. Pattern for Miura-ori (a) Crease pattern of Miura-ori [2]; (b) Semi-folded Miura-ori model

The folding pattern of the miura-ori can be approximated as a combination of rotational joints and rigid planes, as the paper pieces only rotate about the creases and the paper neither stretches nor compresses in the entire process of the motion. This pattern is used for the compression of antennas and solar panels of satellites [3], as the plane of antennas and solar panels needs to be folded and stored into the body of the rocket, which has a much smaller diameter and could be easily deployed while sent into its position.

Although the Miura-ori can fulfil this task, there are some circumstances under which some properties that may be ideal in other applications need to be removed. In the case of the miura-ori, these include the five properties that the mechanism obtains: crease orientation, crease alignment, developability, flat-foldability, and rectilinearity [4]. By removing one characteristic at a time, the structure of the mechanism is altered slightly, and the resulting design can be applied for a greater range of various demands.

By ridding each one of the five design characteristics of the miura-ori, the corresponding parameters that are needed to determine each specific design are also altered. There are also some methods to combine designs of different kinds of miura-ori in order to obtain more general designs and further limit or eliminate the motion features of the mechanism through piecewise incorporation [4].

In Section 2, the quantitative parameters of the five derivatives are validated by the construction of physical models and comparing the measured data with the theoretical values. In Section 3, studies on multi-layered miura-ori structures as well as general curved structures, are summarized, as they could provide various practical uses [5]. The limitations of current studies as well as the possibilities of multi-layered derivatives, are discussed. In Section 4, the validity of the parameters and possible future extensions are concluded.

2. Theoretic Review and Analysis

In the paper by You *et al.*, five derivatives of the miura-ori were proposed, each removing one geometric characteristic of the original fold to form a three-dimensional structure [4]. Based on the altered geometrical characteristics and layout, the relationship between the parameters can be calculated. The equations of each design are all given in the paper. Although the paper mentioned that the parameters are proven through a specific model and the process of calculation is also listed and explained, by using models with different parameters, the equations can be further validated or falsified.

2.1. Arc Pattern

The arc pattern is formed by reversing the crease orientation alternately. Therefore, the basic pattern of the model is no longer parallelograms but isosceles trapezoids, as shown in Fig. 2.

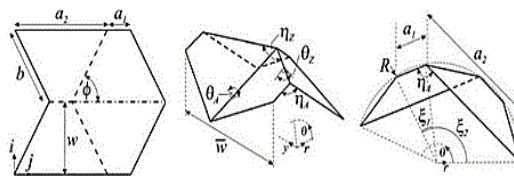


Figure 2. Arc pattern geometry [4]

When the model is completely folded, the angles:

$$\theta_A = \theta_z = \eta_z = 0,$$

the angles have the determined relationship [4]:

$$\eta_A = \cos^{-1}(\sin^2\varphi \cos\theta_z - \cos^2\varphi) = \cos^{-1}(\sin^2\varphi - \cos^2\varphi)$$

The model is designed such that:

$$\varphi = \frac{\pi}{3}$$

Hence there is:

$$\eta_A = \cos^{-1}\left(\sin^2\frac{\pi}{3} - \cos^2\frac{\pi}{3}\right) = \frac{\pi}{3}$$

The above parameters can be proven to be consistent with any one of the three following equations [4]:

$$\eta_z = \cos^{-1}(\sin^2\varphi + \cos^2\varphi)$$

$$L.H.S. = 0, R.H.S. = \cos^{-1}(1) = 0 = L.H.S.$$

$$or: (1 + \cos\eta_z)(1 - \cos\eta_A) = 4\cos^2\varphi$$

$$L.H.S. = (1 + \cos 0)\left(1 - \cos\frac{\pi}{3}\right) = 2 \times \frac{1}{2} = 1, R.H.S. = 4\cos^2\frac{\pi}{3} = 1 = L.H.S.$$

$$or: \bar{w} = b \cdot \sin\frac{\eta_z}{2} = \frac{w \cdot \sin\frac{\eta_z}{2}}{\sin\varphi}$$

$$Since \bar{w} = 0, R.H.S. = 0 = L.H.S.$$

Further calculations can lead to the final validation data:

$$\xi_1 + \xi_2 = 2(\pi - \eta_A) = 2 \times \frac{2\pi}{3}$$

$$\therefore when \xi_1 = \frac{2\pi}{9}, \xi_2 = \frac{10\pi}{9}, \xi_1 + \xi_2 = \frac{4\pi}{3}$$

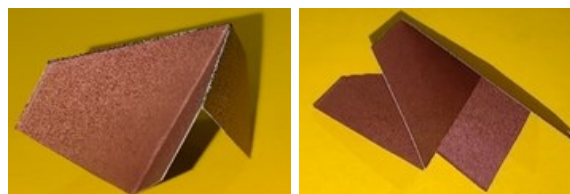
$$Let a_1 = 2.1,$$

$$a_2 = 6.0,$$

$$R_1 = \frac{2.1}{2 \cdot \sin\frac{40^\circ}{2}} = 3.1$$

$$R_{measured} = \frac{2.1}{2 \cdot \sin\frac{40^\circ}{2}} = 3.1$$

By making a physical model, the value that was measured was also 3.1 centimetres. This proves the theory to be coherent with the reality. The complete folding pattern is shown in Fig. 3.



(a)

(b)

Figure 3. Arc model folding pattern, from developed to folded

2.2. Arc-Miura Pattern

Similar to the previous pattern, the Arc-Miura pattern is formed by altering the zigzag side of the parallelograms alternately. Instead of inverting the orientation, the Arc-Miura pattern is formed by altering the alignment of the creases. That is to say, the parallel sides are no longer parallel with all of the others, rather alternately, as shown in Fig. 4.

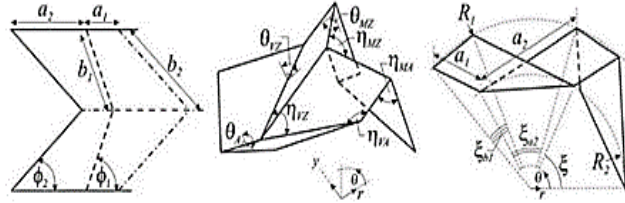


Figure 4. Arc-miura pattern geometry [4]

Therefore, the following equations can be established:

$$(1 + \cos\eta_{mZ})(1 - \cos\eta_{mA}) = 4\cos^2\varphi_1$$

$$\cos\eta_{mA} = \sin^2\varphi_1\cos\theta_{mZ} - \cos^2\varphi_1$$

$$\cos\eta_{mZ} = \sin^2\varphi_1\cos\theta_{mA} + \cos^2\varphi_1$$

$$(1 + \cos\eta_{vZ})(1 - \cos\eta_{vA}) = 4\cos^2\varphi_2$$

$$\cos\eta_{vA} = \sin^2\varphi_2\cos\theta_{vZ} - \cos^2\varphi_2$$

$$\cos\eta_{vZ} = \sin^2\varphi_2\cos\theta_{vA} + \cos^2\varphi_2$$

Where η and θ refer to the angle subtended by the edges and surfaces respectively. m and v refer to the surfaces with the angles φ and $(\pi - \varphi)$ as angles respectively.

First, the parameters that determine the size and shape of the shape are calculated.

$$\text{Let } \varphi_1 = \frac{\pi}{3}, \varphi_2 = \frac{\pi}{6},$$

$$\text{Since } b_1\sin\varphi_1 = b_2\sin\varphi_2,$$

$$\sqrt{3} \cdot b_1 = b_2$$

$$\text{Since } a_2 + b_1\cos\varphi_1 = a_1 + b_2\cos\varphi_2$$

$$\therefore a_2 - b_1 = a_1$$

For ease of calculation and construction,

$$\text{Let } b_1 = 1, b_2 = \sqrt{3}, a_1 = 1, a_2 = 2$$

When the structure is fully deployed, it can be obtained that:

$$\eta_{mZ} = \eta_{vZ} = 0$$

Substituting the values into the equations above:

$$(1 + 1)(1 - \cos\eta_{mA}) = 4 \cdot \frac{1}{4}$$

$$\eta_{mA} = \frac{\pi}{3}$$

$$\frac{1}{2} = \frac{3}{4}\cos\theta_{mZ} - \frac{1}{4}$$

$$\theta_{mZ} = 0$$

$$1 = \frac{3}{4} \cos \theta_A + \frac{1}{4}$$

$$\theta_A = 0$$

$$(1 + 1)(1 - \cos \eta_{vA}) = 4 \cdot \frac{3}{4}$$

$$\eta_{vA} = \frac{2\pi}{3}$$

$$-\frac{1}{2} = \frac{1}{4} \cos \theta_{vZ} - \frac{3}{4}$$

$$\theta_{vZ} = 0$$

Finally, using the sixth equation, the validity of the above calculations can be examined:

$$\cos \eta_{vZ} = \sin^2 \varphi_2 \cos \theta_A + \cos^2 \varphi_2$$

$$L.H.S. = 1, R.H.S. = \frac{1}{4} \cdot 1 + \frac{3}{4}$$

$L.H.S. = R.H.S.$, the calculations are consistent with each other.

The final parameters are calculated from the side view, when a circular shape is formed:

$$\xi = \eta_{vA} - \eta_{mA} [4] = \frac{2\pi}{3} - \frac{\pi}{3} = \frac{\pi}{3}$$

$$R_1 = \sqrt{\frac{a_1^2 + a_2^2 - 2a_1a_2 \cos \eta_{vA}}{2(1 - \cos \xi)}} = \sqrt{7}$$

$$R_2 = \sqrt{\frac{a_1^2 + a_2^2 - 2a_1a_2 \cos \eta_{mA}}{2(1 - \cos \xi)}} = \sqrt{3}$$

The value chosen for validation is η_{vA} , which in the model made is taken to be $\frac{29\pi}{45}$. The divergence is about 3.3%, which is less than 5% and within the acceptable range of random error incurred by uncertainties in the folding process of the model as well as the thickness and deformation of a real piece of paper instead of an ideal material. The model and its folding pattern are shown in Fig. 5.

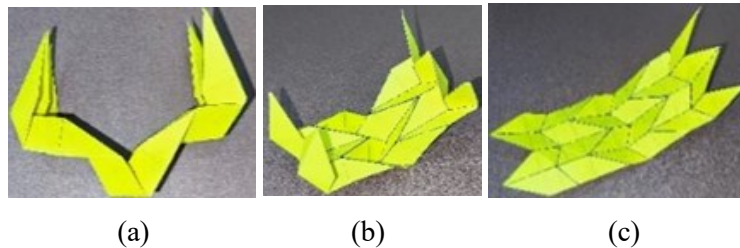


Figure 5. Arc-miura model folding pattern, from developed to folded

2.3. Non-Developable Pattern

The non developable pattern is formed by eliminating the developability of the folding pattern. That is to say, the pattern cannot be fully deployed to form a flat surface. Therefore, it cannot be folded from a flat piece of paper either. Instead, it is formed by connecting two pieces of paper using intermediate pieces that are glued onto the edges of the units. This makes the pattern fundamentally different from the original fold, as it is no longer origami, but kirigami. However, the pattern can still make connections to the original design, as shown in the diagram above in Fig. 6.

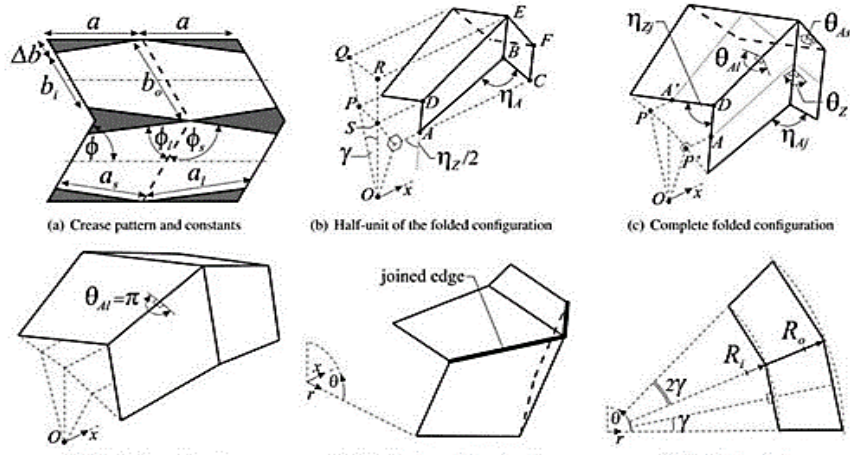


Figure 6. Non-developable pattern geometry [4]

The shaded region is cut out, forming two symmetrical units, whose corresponding sides are connected together. The following equations can be established based on geometric and trigonometric deductions [4]:

$$\begin{aligned}
 (1 + \cos\eta_Z)(1 - \cos\eta_A) &= 4\cos^2\phi \\
 \cos\eta_A &= \sin^2\phi\cos\theta_Z - \cos^2\phi \\
 \tan\gamma &= \frac{\Delta b \sin \frac{\eta_Z}{2}}{a \cos \frac{\eta_Z}{2}} \\
 \cos\eta_{Zj} &= 1 - \sin^2 \frac{\eta_Z}{2} (1 + \cos 2\gamma) \\
 \cos\theta_{Ai} &= \frac{\cos\eta_{Zj} - \cos^2\phi_l}{\sin^2\phi_l} \\
 \cos\theta_{As} &= \frac{\cos\eta_{Zj} - \cos^2\phi_s}{\sin^2\phi_s} \\
 R_i &= \frac{b_i \sin \frac{\eta_Z}{2}}{2\sin\gamma} \\
 R_o &= \frac{b_o \sin \frac{\eta_Z}{2}}{2\sin\gamma}
 \end{aligned}$$

Where the quantities with footnote l and s are quantities corresponding to the longer side and shorter side of the cutout respectively, while the quantities with additional footnote j refer to the quantities formed by the “complete” units, and the quantities without are those formed by “half” units, or the reference lines that are parallel to each other.

Just as in the previous layouts, a specific layout is used for both theoretical deduction and physical model validation. In this case, the specified parameters for the shape, and position of the model are as follows:

$$\begin{aligned}
 \text{Let } \phi &= \frac{\pi}{3}, \Delta b = a, \text{ hence there are } \phi_1 = \frac{\pi}{6}, \phi_2 = \frac{\pi}{3} \\
 \text{When } \cos\eta_A &= \frac{1}{2}, \text{ or } \eta_A = \frac{\pi}{3} \\
 \text{By (1), } \cos\eta_Z &= 1, \eta_A = \pi
 \end{aligned}$$

Using the data obtained in the above equations, they are consequently substituted into the rest of the eight equations above:

$$\begin{aligned} \tan \gamma &= \frac{\Delta b}{a} \times \frac{1}{\frac{\sqrt{2}}{2}} = \frac{2}{\sqrt{3}} \\ \cos \eta_{zj} &= 1 - 1^2 \times \left(1 + \left(-\frac{1}{7} \right) \right) = \frac{1}{7} \\ \cos \theta_{Al} &= \frac{\frac{1}{7} - \frac{3}{4}}{\frac{1}{4}} = -\frac{17}{7} \\ \cos \theta_{As} &= \frac{\frac{1}{7} - \frac{1}{4}}{\frac{3}{4}} = -\frac{1}{7} \end{aligned}$$

After determining the parameters a and b , the final value, which is R_i , the inner radius of the final pattern when viewed from the side.

$$R_i = \frac{(b - 2a) \times 1}{2 - \frac{2}{\sqrt{7}}} \approx 0.66(b - 2a) \quad (20)$$

When $a = 2, b = 6, R_i \approx 1.32$

The value measured in the physical model is 1.2 centimetres, an about 9% deviation from the theoretical value. Considering the imperfections of the material and the volume of the hinges that are neglected in the calculations, as well as the shear movements of the hinges as they are made from paper, the deviation can be accepted as within the random error range of the handmade paper model, shown above in Fig. 7.

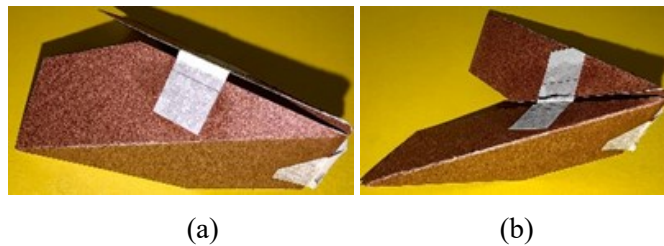


Figure 7. Non-developable model folding pattern, from developed to folded position

2.4. Non-Flat-Foldable Pattern

The pattern is formed by eliminating the flat foldability of the pattern. That is to say, when the pattern is fully folded, the formed result is no longer a flat piece, but rather a structure with thickness [6,7]. Similar to the previous design, the non-flat-foldable pattern is formed by altering the connecting pieces between units, as shown in Fig. 8 below.

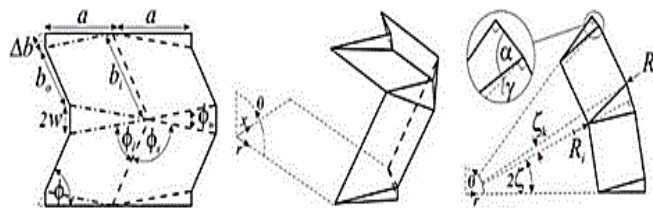


Figure 8. Non-flat-foldable pattern geometry [4]

The following equations can be derived from geometric and trigonometric analysis. Some are very similar to those in the previous layout as these two are very similar, as shown below [4]:

$$(1 + \cos\eta_z)(1 - \cos\eta_A) = 4\cos^2\phi$$

$$\tan\gamma = \frac{\Delta b \sin \frac{\eta_z}{2}}{a \cos \frac{\eta_A}{2}}$$

$$W = \Delta b \sin\phi$$

$$\cos\alpha = \frac{w \cos\gamma}{a \cos \frac{\eta_A}{2}}$$

$$\zeta = \frac{\pi}{2} - \gamma - \alpha$$

$$R_i = \frac{b_i \sin \frac{\eta_z}{2}}{2 \sin \xi}$$

$$R_0 = \sqrt{\left(R_i + \frac{a \cos \frac{\eta_A}{2} \sin\alpha}{\cos\gamma} \right)^2 + w^2}$$

$$\sin \xi_k = \frac{w}{R_0}$$

Here, W refers to the width of the intermediate connecting pieces while ξ refers to the angle subtended at the centre.

The shape and position of the model are specified, and the following values can be determined by substituting the variables in the equations:

$$\text{Let } \phi = \frac{\pi}{3}, \text{ when } \eta_z = \frac{\pi}{3}, \text{ by (1), } \cos\eta_A = \frac{1}{3}.$$

$$\tan\gamma = \frac{\Delta b \frac{1}{2}}{a \cos \frac{\eta_A}{2}}$$

$$\cos^2 \frac{\eta_A}{2} - \left(1 - \sin^2 \frac{\eta_A}{2} \right) = \cos\eta_A = \frac{1}{3}$$

$$\therefore \cos \frac{\eta_A}{2} = \frac{\sqrt{2}}{\sqrt{3}}, \tan\gamma = \frac{\Delta b}{a} \cdot \frac{\sqrt{3}}{2\sqrt{2}}$$

To obtain a specific value, the ratio of Δb and a are determined.

$$\text{when } \Delta b \text{ is taken as } \frac{1}{2}a, \tan\gamma = \frac{\sqrt{3}}{2\sqrt{2}}$$

$$\cos\alpha = \frac{\frac{\sqrt{3}}{2} \cdot \frac{1}{2}a \cdot \frac{4\sqrt{2}}{\sqrt{35}}}{a \cdot \frac{\sqrt{2}}{\sqrt{3}}} = \frac{3}{\sqrt{35}}$$

$$R_i = \frac{b_i \cdot \frac{1}{2}}{2 \cdot \cos(\alpha + \gamma)} = \frac{35b_i}{48\sqrt{2} - 4\sqrt{78}}$$

$$R_0 = \sqrt{\left(\frac{35b_i}{48\sqrt{2} - 4\sqrt{78}} + \frac{\sqrt{26}a}{4\sqrt{3}} \right)^2 + \frac{9}{16}a^2}$$

By determining the specific parameters, the value can be obtained:

$$\text{When } a = 2, b_i = 2\sqrt{3}, R_0 \approx 4.02$$

The model made measures a value of around 7% deviation, at 4.3 centimeters. When considering the imperfections in the model making process and deviations in the measuring process, this is still within the acceptable range of random error, and hence could validate the theory. The model and its folding pattern are shown in Fig. 9 below.

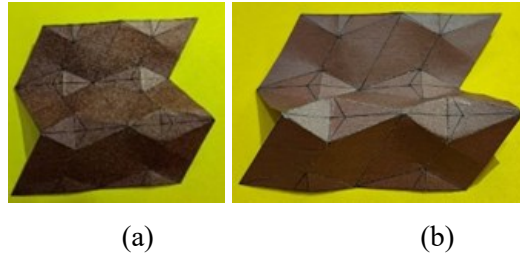


Figure 9. Non-flat-foldable model folding pattern, from developed to folded

2.5. Tapered Miura Pattern

The final pattern is the tapered miura pattern. It is formed by removing the rectilinearity of the original pattern. That is to say, the lines along the longitudinal direction of the pattern are no longer parallel to each other, but instead meet at a point. Therefore, the other sides are also no longer of equal lengths. Like the above, the model is shown in Fig. 10.

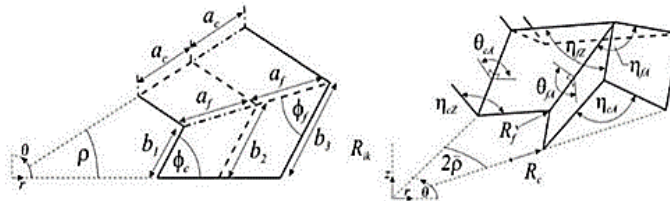


Figure 10. Tapered miura pattern geometry [4]

Based on its geometry, the following equations can be established:

$$\varphi_f = \varphi_c - \rho \quad (30)$$

$$a_c = \frac{a_f \cdot \sin \varphi_f}{\sin \varphi_c} \quad (31)$$

$$\cos \eta_{cZ} = \sin^2 \varphi_c \cos \theta_{cA} + \cos^2 \varphi_c$$

$$\cos \eta_{cA} = \sin^2 \varphi_c \cos \theta_{cZ} + \cos^2 \varphi_c$$

$$(1 + \cos \eta_{cZ})(1 - \cos \eta_{cA}) = 4 \cos^2 \varphi_c$$

$$\cos \eta_{fZ} = \sin^2 \varphi_f \cos \theta_{fA} + \cos^2 \varphi_f$$

$$\cos \eta_{fA} = \sin^2 \varphi_f \cos \theta_{fZ} - \cos^2 \varphi_f$$

$$(1 + \cos \eta_{fZ})(1 - \cos \eta_{fA}) = 4 \cos^2 \varphi_f$$

Specific parameters are substituted into the calculations in order to get specific parameters for calculations:

$$\text{When } \varphi_f = \frac{\pi}{6}, \varphi_c = \frac{\pi}{3}, \rho = \frac{\pi}{6},$$

$$a_c = \frac{a_f \cdot \frac{1}{2}}{\frac{\sqrt{3}}{2}} = \frac{\sqrt{3}}{3} \cdot a_f$$

$$\begin{aligned}
 &\text{When } \eta_{cZ} = 0 \\
 &1 = \frac{3}{4} \cos \theta_{cA} + \frac{1}{4} \\
 &\theta_{cA} = 0 \\
 &2(1 - \cos \eta_{cA}) = 4 \cdot \frac{1}{4} \\
 &\eta_{cA} = \frac{\pi}{3} \\
 &\frac{1}{2} = \frac{3}{4} \cos \theta_Z - \frac{1}{4} \\
 &\theta_Z = 0 \\
 &\cos \eta_{fZ} = \frac{1}{4} \cdot 1 + \frac{3}{4} \\
 &\eta_{fZ} = 0 \\
 &\cos \eta_{fA} = \frac{1}{4} \cdot 1 - \frac{3}{4} \\
 &\eta_{fA} = \frac{2\pi}{3}
 \end{aligned}$$

The final equation can be used for validation of the above calculations:

$$\begin{aligned}
 &(1 + \cos \eta_{fZ})(1 - \cos \eta_{fA}) = 4 \cos^2 \varphi_f \\
 &L.H.S. = (1 + 1) \left[1 - \left(-\frac{1}{2} \right) \right] = 3, R.H.S. = 4 \cdot \frac{3}{4} = 3, \\
 &\therefore L.H.S. = R.H.S, \text{ the calculations are consistent}
 \end{aligned}$$

Since the aforementioned zigzag lines are also of unequal lengths, there is a relationship for the value of those as well:

$$b_j = \frac{b_1 + (j - 1) \cdot a_c \cdot \sin \rho}{\sin \varphi_f} \quad \forall j \geq 2$$

The measured result is the quantity η_{fA} , which was obtained to be $\frac{25\pi}{36}$, a 4% deviation from the theoretical value. The deviation is less than 5% and within the acceptable range of random error incurred by uncertainties in the folding process of the model as well as the thickness and deformation of a real piece of paper instead of an ideal material. The model made is shown above in Fig. 11.

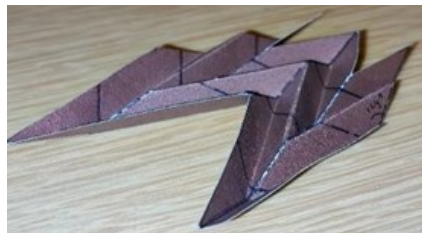


Figure 11. Tapered Miura model folding pattern, from developed to folded

3. Further Discussions & Possible Extensions

The above calculations and experiments validated the theories and parameters for the five derivatives. The following part discusses two possible use for such a pattern, which is to accommodate curved or doubly curved surfaces. The possibility of constructing a multi-layered structure is also discussed.

3.1. Work on More General Curved Miura-ori Structures

The above is work done in already existing works, which present a method of connecting the basic miura-ori pattern. However, the result formed only possesses a flat layout that is identical to the original pattern. Therefore, in circumstances where such a design is not satisfactory, but a curved structure or circular structure is needed, the design based on the first-derivatives of the miura-ori pattern can be formed.

The overall guidelines of the altered design are identical: the layers must be connected so that all creases are collinear, and that motion of each individual layer must be guaranteed. Hence, some details of the designs are to be altered. For example, for arc pattern and arc-miura pattern, the different layers cannot be identical; instead, the radius of the folded structure at the optimal position must increase along the radial direction of the pattern, away from the centre of the curve. The resulting pattern can form curves along the stress-bearing surface, if based on the first two types of derivatives; it can also form curves normal to the stress-bearing surface, if using the fifth type of derivative introduced.

There have been studies made to accommodate these aforementioned circumstances. One solution proposed is by using miura-ori based structures. These structures are not first-derivatives, but instead doubly curved or obtaining single or double curved target surfaces [8] [9]. There have been mathematical deductions based on the geometry and layout of the design, and 3D modelling results also comply with the deductions. The design can be used to provide internal support for objects of irregular layout, and an algorithm is proposed to optimize the structure layout while preserving the characteristics of the original miura-ori structure mentioned above. For example, such an algorithm is used for designing structures providing internal support for standardized airfoils. However, the algorithm does not always derive a valid result, and the number of vertexes are limited to avoid over-constraint. Hence, in the process of forming larger structures, no generalized rule was found and instead empirical models are still needed.

Another possibility proposed by You.*et.al.* is piecewise connection of first derivatives to form structures with certain geometric characters removed [4]. In this process, a more general and not necessarily consistent curvature can be obtained.

3.2. Multi-layered Structure based on the Miura-ori Pattern

The multi-layered structures of the miura-ori fold are formed by overlapping the identical miura-ori folds over each other, one on top of the other. They are rotated about the horizontal axis. Therefore, the number of creases that overlap each other is maximized. Hence, the structure can be fixed at the greatest level.

The multi-layered structures not only possess the foldable characteristics of the original structure, it also gains new characteristics in the process of stacking. Since the layout is self-repetitive in all three dimensions, the layout can be viewed as a type of metamaterial. That is to say, the layout can be repeated indefinitely to form a specific three-dimensional layout and possesses properties that are not obtained by materials that are formed naturally [3]. The multi-layered miura-ori structure obtain a low-density, foldable characteristic while also being able to be used for energy absorption with adjustable stiffness.

As is the case in the previous section, a physical model is made for the validation of this theory. In this case, a quantitative approach is not taken, as the sole goal is to validate the property of the multi-layered design. Three identical miura-ori patterns are made, and two of them are connected together to form the multi-layered structure in the aforementioned fashion. A ceramic weight is placed at the centre of the two structures. It was observed that the single layered mechanism deployed under pressure while the multi-layered structure retained its original shape and presented no obvious deformations. This

proves that by constructing a multi-layered structure, stiffness can be obtained that is greater than that of the material-inherent stiffness.

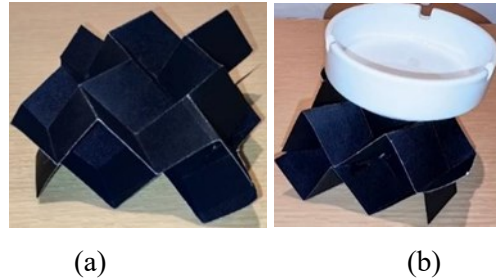


Figure 12. Multi-layered Miura-ori Structure Demonstration. (a) Multi-layered miura model folded pattern. (b) Behavior under load of a ceramic weight

3.3. Discussions on Multi-layered Structure Based on the First-derivatives of the Miura-ori Pattern

The above is work done in already existing works, which present a method of connecting the basic miura-ori pattern. However, the result formed only possesses a flat layout that is identical to the original pattern. Therefore, in circumstances where such a design is not satisfactory, but a curved structure or circular structure is needed, the design based on the first-derivatives of the miura-ori pattern can be formed.

The overall guidelines of the altered design are identical: the layers must be connected so that all creases are collinear, and that motion of each individual layer must be guaranteed. Hence, some details of the designs are to be altered. For example, for arc pattern and arc-miura pattern, the different layers cannot be identical; instead, the radius of the folded structure at the optimal position must increase along the radial direction of the pattern, away from the centre of the curve. The resulting pattern can form curves along the stress-bearing surface, if based on the first two types of derivatives; it can also form curves normal to the stress-bearing surface, if using the fifth type of derivative introduced.

3.4. Limitations & Possibilities for Future Studies

In the passage above, possibilities for both generalized curve structures as well as multi-layered structures are discussed.

For the generalization of curved structures, the algorithm can only cover small-scaled designs, and over-constraint cannot be represented in its calculations. Basic models or general guidelines for the design and optimization of curved folds could be a direction for future work.

The multi-layered design currently only spans over the basic design and kirigami structures [10], and although the structures are optimized through mathematical modelling based on geometrical properties and material properties, and physical simulations of the folding process are also conducted, studies on multi-layered derivatives can be a topic to be discussed in the future.

4. Conclusions

In the work above, we managed to validate the five first-derivatives of the miura-ori fold and the equations of each layout by making physical models with specific parameters and measuring a specific data when the model is at a specific point on the deployment process. The equations are validated by comparing the measured values and the ones obtained through calculations.

Further discussions on curved miura-ori folds and multi-layered first-derivatives are both conducted through summarizing the latest discoveries as well as possible extensions. Further work could be made to fill the gaps of large-scaled curved miura-ori patterns and curved multi-layered miura-ori structures.

References

- [1] D. Dureisseix, “An overview of mechanisms and patterns with Origami,” *International Journal of Space Structures*, vol. 27, no. 1, pp. 1–14, 2012. doi:10.1260/0266-3511.27.1.1
- [2] “Miura fold,” Wikipedia, https://en.wikipedia.org/wiki/Miura_fold (accessed Aug. 21, 2023).
- [3] X. Xiang *et al.*, “The mechanical characteristics of graded Miura-Ori Metamaterials,” *Materials & Design*, vol. 211, p. 110173, 2021. doi:10.1016/j.matdes.2021.110173
- [4] J. M. Gattas, W. Wu, and Z. You, “Miura-base rigid origami: Parameterizations of first-level derivative and piecewise geometries,” *Journal of Mechanical Design*, vol. 135, no. 11, 2013. doi:10.1115/1.4025380
- [5] K. Miura, “The science of miura-ori,” *Origami 4*, pp. 87–99, 2009. doi:10.1201/b10653-12
- [6] T. Kawasaki, “On the Relation Between Mountain-Creases and Valley-Creases of a Flat Origami,” *Proceedings of the 1st International Meeting of Origami Science and Technology*, pp. 229–237, 1989.
- [7] “Activity 16 exploring flat vertex folds,” *Project Origami*, pp. 165–178, 2006. doi:10.1201/9780429062940-23
- [8] K. Song, X. Zhou, S. Zang, H. Wang, and Z. You, “Design of rigid-foldable doubly curved origami tessellations based on trapezoidal crease patterns,” *Proceedings of the Royal Society A: Mathematical, Physical and Engineering Sciences*, vol. 473, no. 2200, p. 20170016, 2017. doi:10.1098/rspa.2017.0016
- [9] Y. Hu, Y. Zhou, and H. Liang, “Constructing rigid-foldable generalized Miura-ori tessellations for curved surfaces,” *Journal of Mechanisms and Robotics*, vol. 13, no. 1, 2020. doi:10.1115/1.4048630
- [10] X. Zhang *et al.*, “Kirigami-based metastructures with programmable multistability,” *Proceedings of the National Academy of Sciences*, vol. 119, no. 11, 2022. doi:10.1073/pnas.2117649119